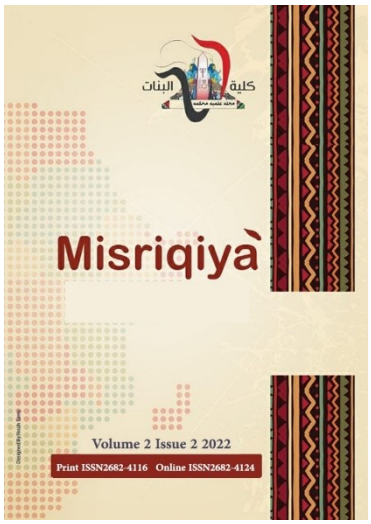

Detection and mapping of land use land cover with Support vector machines SVM-based change monitoring using Landsat and Sentinel-2 data. The case of Quseir, Red Sea

Emad Hawash[1], Adel El-Hassanin[1], Wafaa Amer[2], Alaa EL-Dien EL-Nahry[3], Hala Effat[3]

1.Faculty of African Postgraduate Studies, Cairo University, Egypt
2.Faculty of Regional and Urban Planning, Cairo University, Egypt
3.National Authority of Remote Sensing and Space Sciences, Ministry of Scientific Research, Egypt

Received: 20-5-2022 Revised: 1-9-2022 Accepted: 7-9-2022
Published: 5-10-2022

DOI: **10.21608/MISJ.2022.273084**
https://misj.journals.ekb.eg/article_273084.html

Citation: Hawash, E., El-Hassanin, A., Amer, W., EL-Nahry, A. E., & Effat, H. (2022). Detection and mapping of land use land cover with Support vector machines SVM-based change monitoring using Landsat and Sentinel-2 data. The case of Quseir, Red Sea. *Miṣriqiyā*, *2*(2), 1-30. doi: 10.21608/misj.2022.273084

Abstract

Land use land cover (LULC) mapping and spatial change monitoring are essential to manage the coastal cities and its resources. This study aims to investigate LULC changes of Quseir, a typical small Red Sea coastal city for a long period from 1984 to 2021. Support vector machines (SVMs) classifier and Post classification comparison (PCC) change detection technique were used to analyse two Thematic Mappers (TM), an Enhanced Thematic Mapper plus (ETM+), an Operational Land Imager (OLI) Landsat imagery in addition to a Multi-Spectral Instrument (MSI) Sentinel-2 image cover the study period. Twelve LULC classes have been identified for this study. Accuracy of the classified images and the LULC change were analysed. Along the thirty-seven years, Quseir's urban has increased by nine folds and the green area was increased from nil to 6.10 m2 per person. SVM achieved high accuracy classification results for all the studied images of all sensors, while the MSI, 2021, had the highest accuracy. Through data-resampling, combining Landsat and Sentinel-2 satellite datasets for long-term monitoring studies using PCC resulted in more reliable and accurate outputs. Results obtained from this study will fill the gap of rare LULC maps and spatial change information of Quseir during the past four decades.

Keywords*: Land use land cover change; SVM; PCC; Sentinel-2; Landsat; Quseir Red Sea.*

Detection and mapping of land use land cover with Support vector machines SVM-based change monitoring using Landsat and Sentinel-2 data. The case of Quseir, Red Sea

Emad Hawash (Ph.D.)
Natural Resources Dept.
Faculty of African Postgraduate Studies (FAPS)
Cairo University, Egypt.
Red Sea Sustainability Studies Centre (RSSSC)
al_hawash@yahoo.com

Prof. **Adel El-Hassanin**
Natural Resources Dept.
Faculty of African Postgraduate Studies
Cairo University, Egypt

Prof**. Wafaa Amer**
Urban Planning Dept.
Faculty of Regional and Urban Planning
Cairo University, Egypt

Prof. **Alaa EL-Dien EL-Nahry**
Cont. Training and Teaching Dept.
National Authority of Remote Sensing and Space Sciences (NARSS)
Ministry of Scientific Research, Egypt

Prof. **Hala Effat**
Environment and Land-use Dept.
National Authority of Remote Sensing and Space Sciences (NARSS)
Ministry of Scientific Research, Egypt

10.21608/misj.2022.273084

Received: 20-05-2022
Accepted: 07-09-2022
Published: 05-10-2022

Abstract

Land use land cover (LULC) mapping and spatial change monitoring are essential to manage the coastal cities and its resources. This study aims to investigate LULC changes of Quseir, a typical small Red Sea coastal city for a long period from 1984 to 2021. Support vector machines (SVMs) classifier and Post classification comparison (PCC) change detection technique were used to analyse two Thematic Mappers (TM), an Enhanced Thematic Mapper plus (ETM+), an Operational Land Imager (OLI) Landsat imagery in addition to a Multi-Spectral Instrument (MSI) Sentinel-2 image cover the study period. Twelve LULC classes have been identified for this study. Accuracy of the classified images and the LULC change were analysed. Along the thirty seven years, Quseir's urban has increased by nine folds and the green area was increased from nil to 6.10 m^2 per person. SVM achieved high accuracy classification results for all the studied images of all sensors, while the MSI,

2021, had the highest accuracy. Through data-resampling, combining Landsat and Sentinel-2 satellite datasets for long-term monitoring studies using PCC resulted in more reliable and accurate outputs. Results obtained from this study will fill the gap of rare LULC maps and spatial change information of Quseir during the past four decades.

Key words:
Land use land cover change; SVM; PCC; Sentinel-2; Landsat; Quseir Red Sea.

1. Introduction

As a home to inhabitants and home to resource-based and industrial-based activities, coastal cities are of great socio-economic importance and one of the sustainability solutions that are suitable and essential for the current and future generations. Land use land cover (LULC) mapping and LULC change detection have been shown as primary management needs that can be used in different monitoring and management applications at different levels. More importantly, LULC changes on any land surface are among the main influences that driving the changes of the global environment by influencing the climate, ecosystem and services in recent times and expected to extend into future (e.g., Lambin et al., 2014; Steffen, 2004; Srivastava et al., 2012; Turner et al., 1993; Walker and Steffen,1999). Further, sustainable development and its 11 $^{th.}$ Goal -Sustainable cities and communities can be achieved /supported by monitoring the processes of spatial change of the cities/communities around the world using all available tools and techniques. Moreover, using consecutive LULC maps of a given time distance as a basis to analyse local/global sustainability indicators can provide measurable information on the progress of the city /community towards sustainability.

In Egypt, so far, the desert represents the largest share of its area, leaving only 5% densely populated, while it has ambitious schemes to expand the inhabited area to 22% in the near future (MoHUUC, 2014). The overcrowding in areas and devoid of urbanization in other areas is a complex and unique phenomenon in Egypt along the time. In the 1980s, most of the Red Sea coastal cities (RSCC) in Egypt received influxes of internal migrants seeking socio-economic opportunities in the remote coastal areas with valuable and unique natural resources (Abdel-Aal, 1992; Hawash et al, 2021b). After decades of urban development and receiving internal migration, it is important to obtain spatial

information about Quseir, a typical small RSCC and its surrounds, where the LULC change and subsequent analysis represent the cornerstone.

A very important use of satellite remote sensing is the generation of spatially contiguous, thematic information and inventories of the Earth's surface, along with the detection of land cover changes (Chuvieco, 2020). Since the seventies; Landsat Program has provided valuable remote sensing information that enables the analysis of long-term processes on any given place on Earth. Recently, in June 2015, Sentinel-2 began to provide optical imagery at higher spatial resolution (10/20/60 m) and higher spectral resolutions (13 bands) over land and coastal waters. Sentinel-2 constellation will enhance continuity of Landsat and SPOT like information thanks to the higher revisit frequency and a very large swath (Lambert et al., 2018; USGS, 2019a). The spatio-temporal resolution of Landsat images has been and remains sufficient to support a wide range of scientific and commercial applications while the higher spatial and spectral resolutions of Sentinel-2 will provide data useful for near real-time monitoring and high accuracy outputs as well.

Various image classification methods and change detection techniques have been used to analyse remotely sensed data to maintain robust spatial monitoring tools over the past decades. Change detection is the process of identifying differences in the status of an object by observing it at different dates (Singh, 1989). The goal of change detection (CD) is to compare the spatial representation of two time points to measure changes that occurred in variables of interest and control for changes that occurred in variables that are not (Green et al. 1994). CD is a comparing process between two or more representatives of a variable along the studied period(s), from which the differences (changes) can be identified and analysed. Different CD approaches were categorized by scientists and scholars based on different viewpoints (e.g., Lunetta, 2000, Chan et al., 2001, Lu et al., 2004, Ilsever and Ünsalan, 2012 and Chughtai et al., 2021). In general, change detection techniques include: 1) pre-classification and 2) post-classification comparison (PCC) change detection (Singh, 1989; Lunetta, 1998; Ridd and Liu. 1998; Yuan et al. 1998, 2005 and Peiman, 2011). The accuracy of the change detection largely depends on the accuracy of the two separate classification maps (Jensen, 2015; Singh, 1989). And so, it is important to select an appropriate classifier in order to ensure high-accuracy results for the classified datasets, which accordingly will lead to prevent the accumulation of classification errors generated by PCC (e.g., Hawash et al,

2022a; Singh, 1989). PCC was used in various studies (e.g., Aljenaid et al., 2022; Alawamy et al., 2020; Hawash, 2014; Kamel and Abu El Ella, 2016 and Mandal et al., 2019).

To map LULC, various classification approaches have been developed decades ago. In logic, they ranged from supervised to unsupervised; parametric to nonparametric to non-metric, or hard and soft (fuzzy) classification, or per-pixel, sub-pixel, and prefield (Keuchel et al. 2003, Jensen 2005; Al-doski et al., 2013). Support vector machine (SVM) is one of the most powerful non-parametric classifiers (Hawash et al., 2021a; Huang et al., 2002). The SVM has been developed in the statistical learning theory (Vapnik, 1995). SVM seeks to separate land use-cover classes by finding a plane in the multidimensional feature space that maximizes their separation (Foody and Mathur, 2004). Various studies have used SVM (e.g., Cavur et al., 2019; Hawash et al., 2021a; Izadi et al., 2022; Jumaah et al., 2022 and Zhang et al., 2020).

Previous studies of Quseir that investigated its natural resources and different environmental hazards using remote sensing and GIS include: determining the geomorphological hazard between Safaga and Quseir (e.g., Youssef et al., 2009); analysing the drainage basins between Quseir and Abu Dabbab (e.g., Abdel Ghany, 2015) and assessing water resources in el-Ambagi basin (e.g., Yousif and Sracek, 2016). As most of the RSCC, there are no specific studies that cover LULC mapping, LULC change of Quseir, which consider a main administrative and planning problem when managing the city or measuring its progress towards sustainability.

Four decades ago, due to different socio-economic factors, Quseir has undergone various spatial changes, which has to be investigated to gain lessons and help in developing management scenarios. The main objective of this study is to analyse LULC change of Quseir using remote sensing and GIS during 1984-2021. A combination of Landsat data and Sentinel-2 data was used in this study. More specifically, four kernels of SVMs were compared to obtain different LULC classes. Using PCC, the intensity of the LULC changes along the thirty-seven years was then analysed. Results of this study will support the local understanding on the changes occurred in the city (land use of the urban and green areas) and its surrounds (land cover of the desert and mountainous areas). Also, it will provide useful data for the stakeholders to take better decision to sustain the region.

2. Material and methods

2.1. Study area

Quseir (Fig. 1) is a RSCC that has been a crucial trade route from the days of ancient Egyptian and Roman times to this day. During 1910s and the early 1960, the city was home of phosphate mining and industries in Egypt (Cabassi, 2012). It is a historic coastal city that represents a combination of distinctive aspects of its place, urban fabric, natural content, and the physical humanitarian output. The city contains some famous architectural spots such as the House of Sheikh Tawfiq, the Ottoman Castle of Quseir, the Administration Building of the old phosphate factory and the old City Police department.

Quseir extends for about 28.00 km along the western coast of the Red Sea. The study area lies between UL, 26 ^{o} 11" 39' E., 34^{o} 11" 52' N. and LR, 25 ^{o} 55" 49' E., 34^{o} 28" 22' N. It is connected to Hurghada City (capital of Red Sea Governorate-RSG) (north) and Marsa Alam City (south) by a longitudinal road of 135 km and 140 km, respectively. Also, it is connected with the Nile River by Quseir-Qift road, served by a main port and Marsa Alam international Airport. It was the home of el-Hamarwien port, which was used to export phosphate. Quseir is a single district city that has 51,035 inhabitants, and its basic economic activities are fishing, tourism, mining and quarries (CAPMAS, 2021). Temperature varies between 36-24 °C in summer and 26-19 °C in winter. Precipitation varies between 6-19 mm / annum. The average annual percentage of humidity is 49.0%. Winds direction at the coast is almost northerly and north westerly throughout the year (EMA, 2006).

2.2. General considerations of the study area

Geo-morphologically, the study area can be divided into two parts; the Duwi range (a long sharp ridge) and the coastal plain (no sharp bends or bays and slopes gently seaward) (Salem et al., 2005). Geologically, the study area is part of the Central Eastern Desert of Egypt, where the sedimentary rocks of the area are mainly separable into two divisions: (i) the pre-rifting Cretaceous-Eocene group and (ii) the post-rifting Oligocene and later sediments group (Said, 1992). Wadi Hammamat, Wadi Quseir el-Qadim and Wadi el-Ambagi are of the most famous wadis of the area. Further, coastal sabkha is mainly located in two regions (i) the silted lagoon at Quseir el-Qadim region (north) and (ii) el-Edwa region (south), which are almost bare.

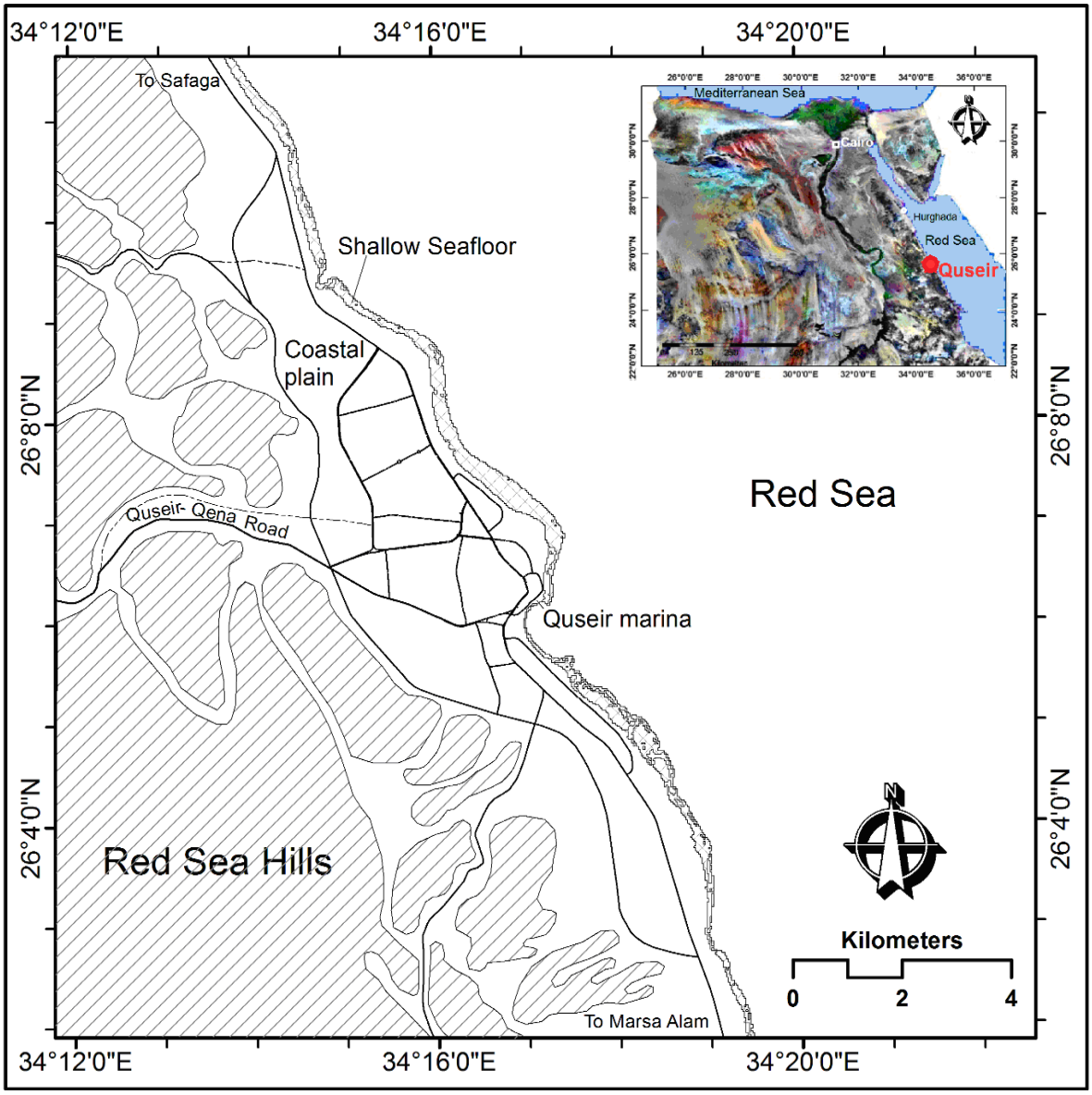

Fig. 1: The study area, extracted from Sentinel-MSI-2A, 2021.

2.3. Datasets and field work

2.3.1. Datasets

When dealing with land and monitoring products extracted from satellite imagery, stakeholders should benefit from both the free-available, long historical archive of Landsat data and the high spatio-temporal resolution of Sentinel-2. In this study, multi-sensor Landsat data (e.g., Thematic Mapper-TM, Enhanced Thematic Mapper plus-ETM+ and Operational Land Imager-OLI) path 174/row 042 and a Sentinel-2 image (Multi Spectral Instrument, MSI),

collected on multiple dates were used. The Landsat datasets were obtained free of charge from the U.S. Geological Survey (USGS): http://earthexplorer.usgs.gov ,while the Sentinel image was obtained from: https://sentinel.esa.int/web/sentinel/sentinel-data-access the Sentinel data access hub. In order to minimize the seasonal effects on the change detection work (e.g., Lillesand et al., 2015), the collected cloud-free images were selected within a single season, i.e. summer. For the Landsat data, analysis of this work used the visible (b1, b2, and b3), NIR (b4) and SWIR (b5 and b7) bands, which are of 30 spatial resolution. Meanwhile, for the Sentinel-2 image, the 10 meters bands i.e. the visible (b2, b3, and b4), the NIR (b8) and the 20 meters bands i.e. SWIR (b11 and b12) were used (Tables 1 and 2). In addition, a topographic map (ESA, 2008) of scale 1:100,000 and a geologic map (EGSMA, 1991) of scale 1:250,000 of Quseir were used as base map, urban and geological references.

2.3.2. Field work.

In this study, field work aims to visually observe the region and to collect region of interests (ROIs) and information from the locals. For Quseir and its surroundings, number of field trips was conducted during August-September 2020 and 2021. By the aid of hard copies of the false colour composite (FCC) images of the current work (1984-2021), ESA-2008 and EGSMA-1991 maps, active Google Earth Pro and Garmin-etrex10 GPS, extensive field surveys were performed. A field sampling sheet covers all the classes was presented. The collected samples of each ROI were separated into two sets: (i) a set for the classification stage and (ii) a set for the accuracy stage (e.g., Hawash et al., 2021 a). Further historical LULC change information was obtained from the locals.

2.4. Approach and Methods

To monitor and analyse change processes in LULC, it is essential to obtain consistent data over a longer period of time and preferably be derived from the same data source while applying the same processing techniques (Verburg, et al., 2011). To fulfil the objectives of this study an integrated remote sensing and GIS approach was adopted. Methodology of this work includes: Landsat and Sentinel image pre-processing, LULC mapping of the studied dates (using four kernels of SVMs) and LULC change analysis in the studied intervals (using PCC) (Fig. 2). The method relies on image processing techniques and analyses using ENVI 5.3, SNAP 9.0 and Arc-GIS 10.6 software.

Table 1: Specification of the used satellite images from different sensors

Satellite	Acquisition date	Sensor	Used bands	Spatial resolution (m)
Landsat 5	02-06-1984	TM	1- 5 and 7	30
Landsat 5	18-09-1994	TM	1- 5 and 7	30
Landsat 7	27-07-2001	ETM+	1- 5 and 7	30
Landsat 8	22-09-2013	OLI	2- 7	30
Sentinel-2	18-08-2021	MSI	2- 4 and 8	10
			and 11-12	20

(Collected by the authors)

Table 2: Band names, wave length, and spatial resolution of the studied images from different sensors (extracted from USGS 2019b and USGS 2019c).

Band Name	Landsat, TM and ETM (USGS, 2019b).	Landsat, OLI (USGS, 2019b).	Sentinel-2, MSI (USGS, 2019 c).
Blue	b1: (0.441-0.514 µm) (30 m)	b2: (0.450 - 0.51 µm) (30 m)	b02: 490 nm (10 m)
Green	b2: (0.519-0.601 µm) (30 m)	b3: (0.53 - 0.59 µm) (30 m)	b03: 560 nm (10 m)
Red	b3: (0.631-0.692 µm) (30 m)	b4: (0.64 - 0.67 µm) (30 m)	b04: 665nm (10 m)
NIR	b4: (0.772-0.898 µm) (30 m)	b5: (0.85 - 0.88 µm) (30 m)	b08: 842 nm (10 m)
SWIR 1	b5: (1.547-1.749 µm) (30 m)	b6: (1.57 - 1.65 µm) (30 m)	b11: 1610 nm (30 m)
SWIR 2	b7: (2.064-2.345 µm) (30 m)	b7: (2.11 - 2.29 µm) (30 m)	b12: 2190 nm (30 m)

TM= Thematic Mapper; ETM+= Enhanced Thematic Mapper plus; OLI= Operational Land Imager; MSI= Multispectral Instrument; NIR= Near-Infrared; SWIR= Short-wave infrared. (Collected by the authors from the mentioned references).

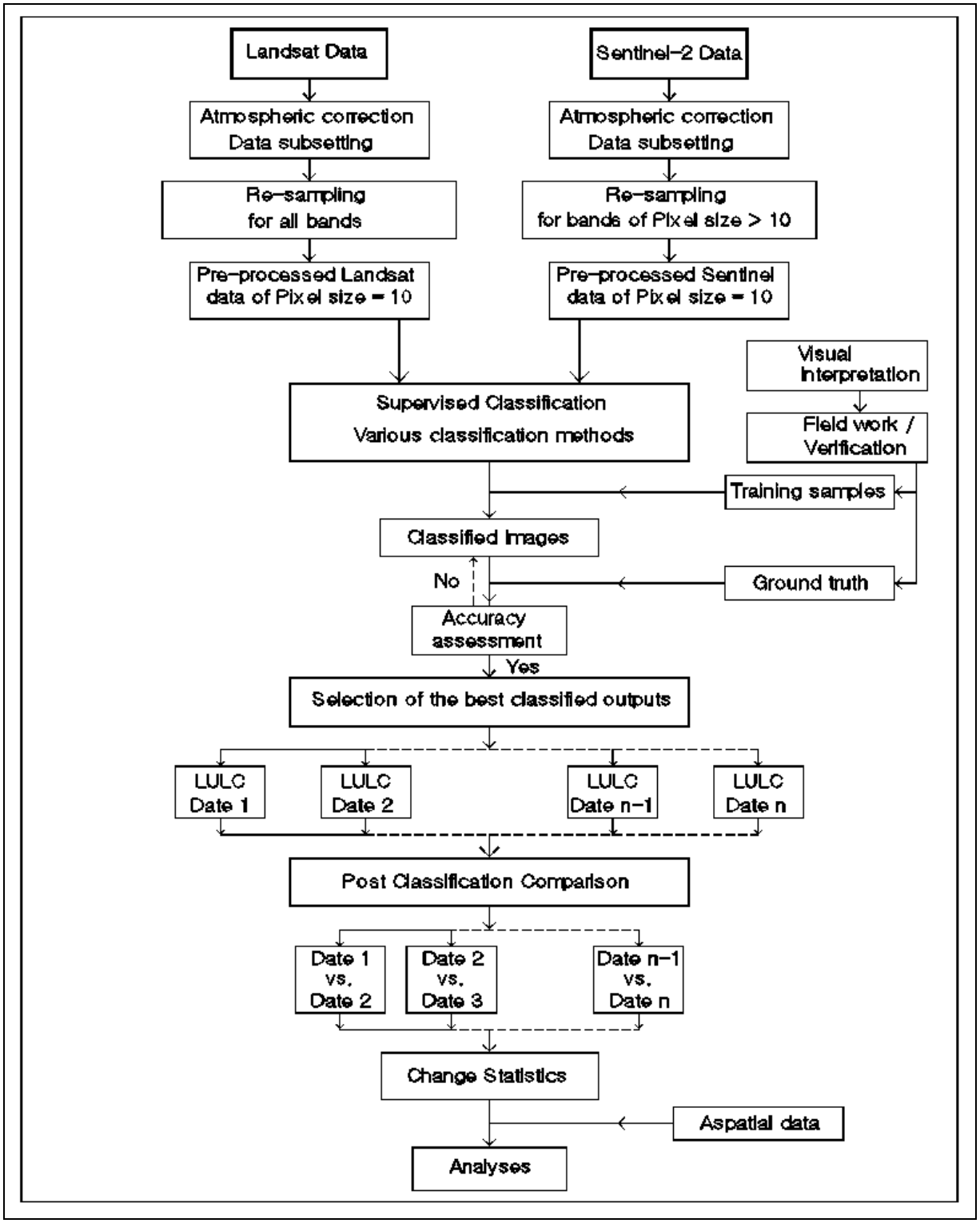

Fig. 2. Methodology of LULC mapping and LULC change procedures (Designed by the authors).

2.4.1. Digital images pre-processing.

For the radiometric characteristics, the Sentinel-2A data has spectral bands very similar to Landsat 8 data (excluding the thermal bands of Landsat 8's Thermal Infrared Sensor), while for the geometric characteristics, Sentinel-2A Level-1C products have similar geometric accuracy as Landsat 8 (USGS, 2019a). From here, in monitoring studies that contains both Landsat and Sentinel-2 data, the OLI scene has two roles: (i) as a main input Landsat data and (ii) as a link between the other Landsat datasets (the historic data) and the Sentinel-2 data.

By the aid of the meta-data of each image, all the original bands of each Landsat image were atmospherically corrected using Fast Line-of-sight Atmospheric Analysis of Spectral Hypercubes, (FLAASH) (e.g., Adler-Golden et al., 1999; Chander et al., 2009; and Ihlen, 2019). All the used Landsat images are ortho-rectified products, World Geodetic System (WGS 84) datum and the Universal Transverse Mercator (UTM) projection system, Zone 36 North.

Essentially, all the images that will be used in the PCC must be co-registered. The OLI-2013 was used as the base file, while the other Landsat images were used as warp file. Number of tie points was used in the nearest neighbour resembling stage. The resulted total RMS Error was 0.014, 0.018, and 0.021 for the TMs, 1984, 1994, and the ETM, 2001, respectively. The OLI-2013 image is indeed geo-referenced with the MSI-2021 (e.g., USGS, 2019a).

The atmospheric correction processor Sen2Cor is a Level-2A processor, which main purpose is to correct single-date Sentinel-2 Level-1C Top-Of-Atmosphere (TOA) products from the effects of the atmosphere in order to deliver a Level-2A Bottom-Of-Atmosphere (BOA) reflectance product (Main-Knorn et al., 2017). In SNAP, using the Thematic Land Processing, the original unzipped Level-1C product MSI was processed in Sen2Cor for atmospheric correction. Eventually, a square of 18×18 kilometre covering the study area was used to extract the subsets of all dates. Data resembling is an important stage in this work. Using majority filter, the pixel size of all Landsat bands was resampled from 30*30 to 10*10 metres. For the Sentinel-2 SWIR layers 11 and 12, they were also resampled from 20*20 to 10*10 metres.

2.4.2. Producing LULC of Quseir

2.4.2.1. SVM for LULC classification

A classical classification algorithm either works straightforward (when the data is linearly separable) or uses kernels (when the data is not linearly separable). A

kernel is a function that transforms the input data to a high-dimensional space so that the data is separable and the problem can be solved in the new space (ENVI Geospatial documentation centre-ENVI GDC). In other words, kernels are used by classification algorithms to solve non-linear classification problems. In this study four kernels of SVMs i.e. Linear, Polynomial, radial basis function-RBF, and Sigmoid will be employed for each image date (Table 3).

When employing SVM and in order to make sure that the entire image is classified, each pixel is restricted to a single category, and no pixels to remain unclassified, some parameters must be carefully set for the used kernels. These parameters include: (i) generic parameters of the algorithm (Gamma parameter and The penalty parameter) and (ii) software specific parameters of the classification process (Pyramid levels, Pyramid reclassification threshold, and Classification probability threshold). In their works, Alganci, 2019, Petropoulos et al., 2010, Petropoulos et al., 2011, and Srivastava et al., 2012 described the use of the suitable values for these parameters when using SVM. Gamma parameter is calculated as the inverse of the number of image bands. It is a reasonable but not a perfect default value (ENVI GDC). The maximum value of the penalty parameter is 100, which is set to force all pixels in the ROI to get together to a class (to avoid misclassification at the training area stage). Compatibly, in order to make the image to be processed at its full spatial resolution, the pyramid parameter is set to a value of zero for all kernels.

Table 3: The common uses SVM kernel functions.

Kernel's Name	Kernel Functions	Reference
Linear	$K(x_i, x_j) = \left\langle x_i^T x_j \right\rangle$	(Vapnik, 1995)
Polynomial	$K(x_i, x_j) = \left\langle x_i^T x_j \right\rangle^d$ or $K(x_i, x_j) = (\left\langle x_i^T x_j \right\rangle + 1)^d$	(Vapnik, 1995)
RBF	$K(x_i, x_j) = \exp\left(-\frac{\left\| x_i - x_j \right\|^2}{2h^2} \right)$ where $h > 0$	(Vapnik, 1995)
Sigmoid	$K(x_i, x_j) = \tanh(\eta(x_i^T x_j) + \theta)$ where η and θ parameter	(Evgeniou, et al., 2000)

(The parameters of the SVM kernel functions are described in ENVI GDC).

Further, to make sure that all of the pixels are assigned to a certain class (category), a classification probability threshold of zero must be used.

2.4.2.2. Image classification

The images of the years 1984/1994/2001 have no available training sites data. The training sites were therefore selected based on the spectral signature of the classes and, in the case of known stable land uses, through comparison with the known LULC in 2013 and 2021. To obtain high-accuracy classification results, the collected ROIs should be examined carefully and the spectral separability between each ROI pairs has to be computed (Hawash et al., 2021a). Jeffries-Matusita (J-M) can compute ROI pairs' separability through values range between 0.00 and 2.00, where values greater than 1.90 indicate that the ROI pairs have good separability (Richards, 2013). In this work, the values of J-M ranged from 2.00-1.90, indicating good separability (e.g., Richards, 2013). After J-M check, the scheme of Quseir LULC classes was organized in its final form. Based on a modified list of Anderson classification system (Anderson et al. 1976), field observations and scheme of Marsa Alam LULC (e.g., Hawash et al, 2021 b), the scheme of Quseir LULC was carried out (Table 4). In this work, using the ROI classification-set of each date, the four SVMs kernels were used to classify the studied images. Then, using the ROI accuracy-set of each date, the confusion matrices were computed (e.g., Congalton and Green, 2019).

2.4.3. Change detection using PCC

The following section presents (i) the procedures used to employ PCC for each consecutive pair of the classified images and (ii) computing PCC accuracy. To allow for comparison of Sentinel-2 and Landsat outputs, the resampling stage was of utmost important for this study. Using the independently classified images of each date, a pixel-based comparison was used to produce quantitative change information. PCC change detection is employed to compute the internal change variations between each consecutive classified pairs. PCC procedures were implemented to obtain change results of the first interval (1984-1994), second interval (1994-2001), third interval (2001-2013) and fourth interval (2013-2021), where four cross tabulation were extracted. For the PCC accuracy, the accuracies of the individuals were used to compute the overall change detection accuracy of each interval (e.g. Stow et al., 1980).

Table 4. LULC scheme of Quseir

No.	Symbol	LULC class	Description
1	Ur	Mixed urban/built-up areas	Residential, commercial, industrial, services, and utilities.
2	Gr	Green area	Parks, private/general green open-areas, botanical gardens, green areas in touristic villages and resorts, golf courses, etc.
3	Mn	Mangrove	Coastal wetland composed of forest and scrub dominated by *Avicennia marina.*
4	S	Sandy areas other than beaches	Sand and silt deposits with spares vegetation.
5	SG	Mixed sand and gravel	Combination of sand, pebble, and gravel-field outcrops
6	Wd	Wadi deposits	Quaternary sediments
7	Sb	Coastal sabkha	A flat salt-encrusted desert that is usually lacks any significant plant cover due to the high concentration of salts and sediments
8	B	Basalt	Basaltic rocks
9	M	Metamorphic	Metamorphic rocks
10	L	Limestone	Limestone rocks
11	Ws	Shallow water	Shallow seafloor
12	W	Water	Sea-water

3. RESULTS AND DISCUSSION

3.1. Classification results

3.1.1. LULC maps and accuracy

Using SVMs, Quseir TM-1984, 1994, ETM-2001, OLI-2013 and MSI-2021 were classified (Fig. 3 and 4) and (Table 5). In small desert coastal cities like Quseir, desert categories are dominated, while green and urban categories are always represented by small areas. The quality of the produced classified images can be evaluated through the accuracy of each classification method (e.g., Lu and Weng, 2007). For this work, all the used SVM kernels attained high overall accuracy (>90.0%) (Table 6). These accuracy results exceeded the needed accuracy percentage for an image to contribute in PCC change detection work (e.g., Anderson et al., 1976).

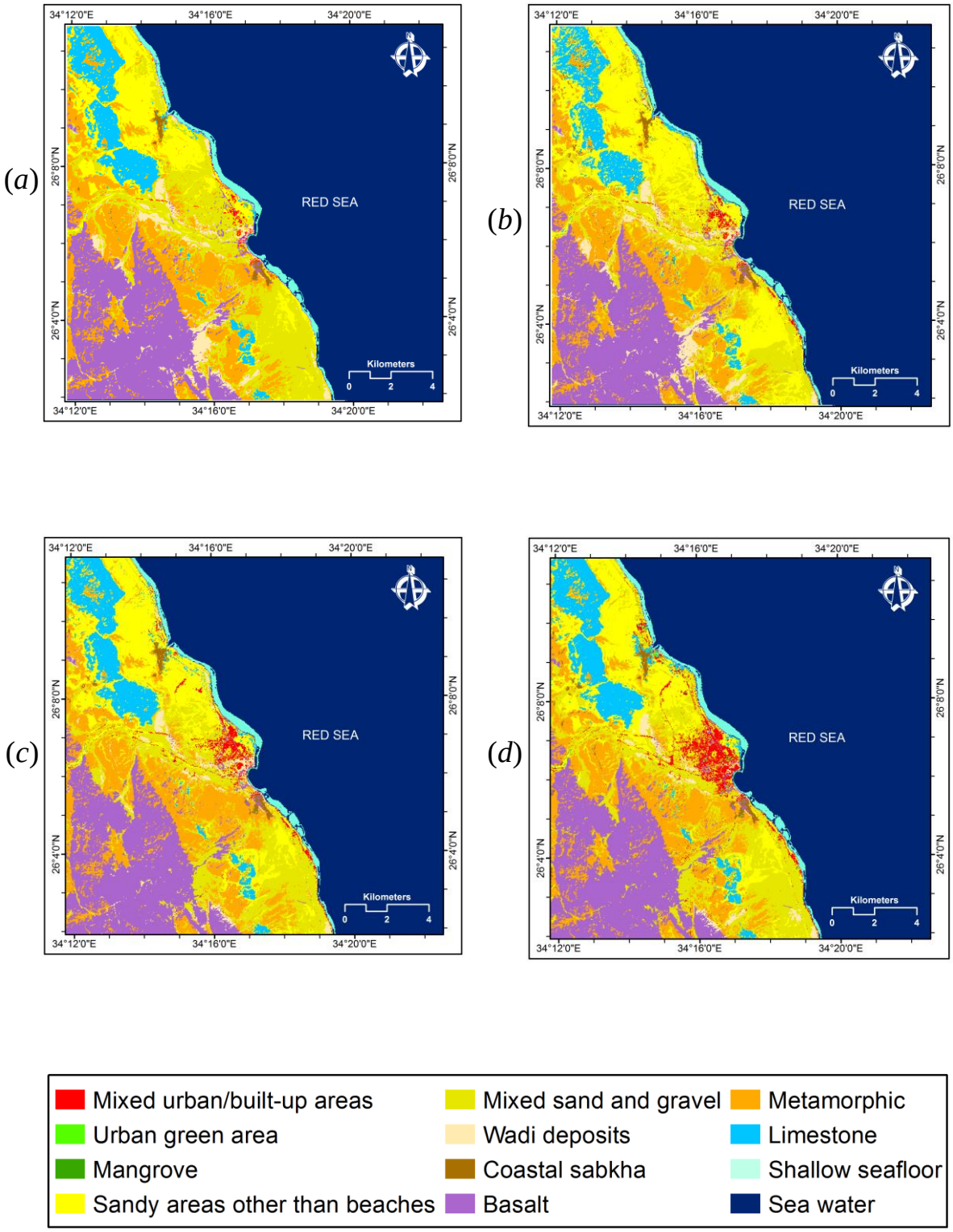

Fig. 3. LULC maps of Quseir, (*a*) 1984, (*b*) 1994, (*c*) 2001 and (*d*) 2013.

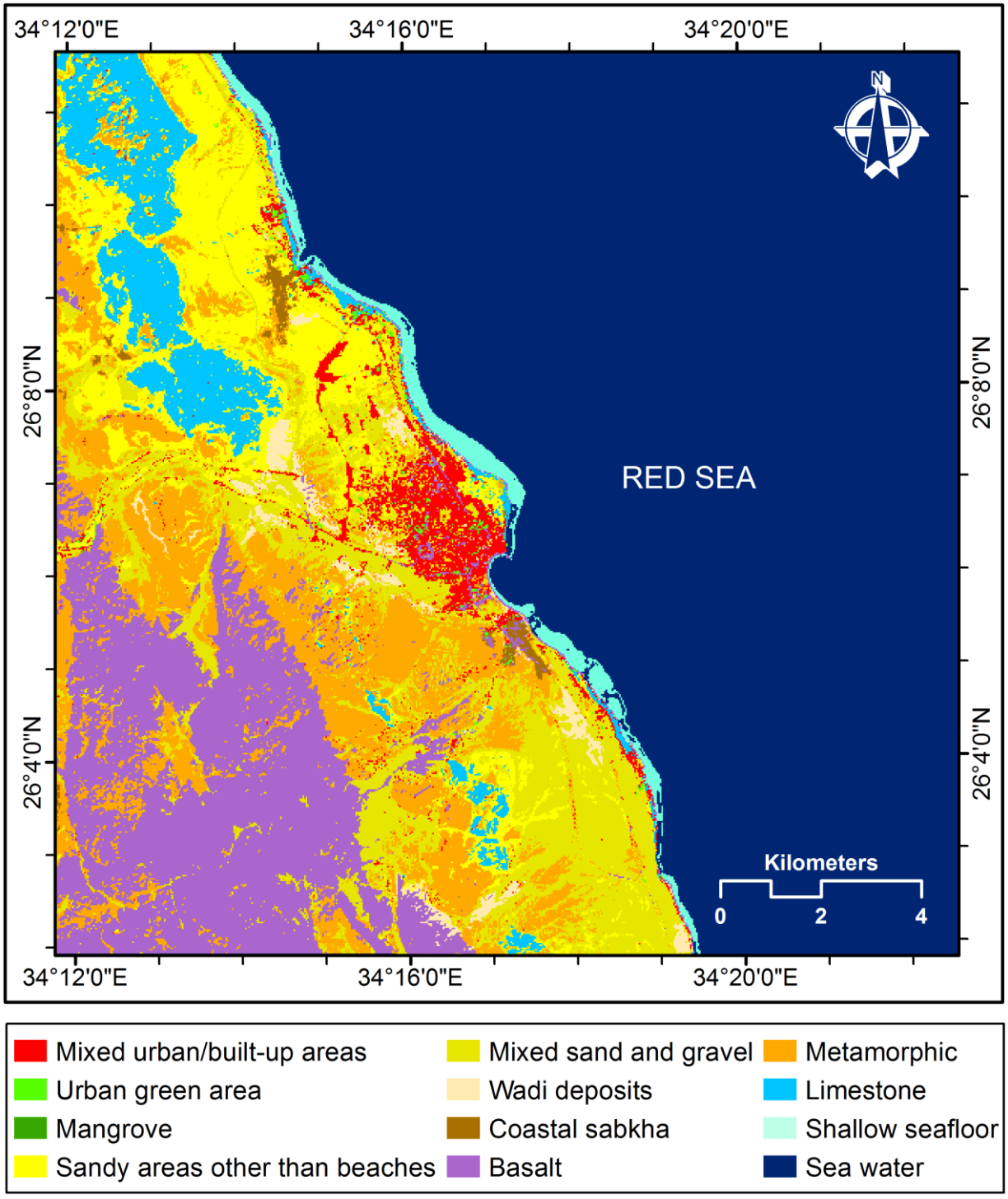

Fig. 4. LULC map of Quseir 2021.

Table 5. LULC areas extracted from classified images of Quseir (1984-2021)

LULC	19 84		19 94		20 01		20 13		20 21	
	Km^2	%	Km^2	%	Km^2	%	Km^2	%	Km^2	%
Ur	0.48	0.15	0.85	0.26	1.79	0.55	3.66	1.13	4.77	1.47
Gr	0	0.00	0.11	0.03	0.15	0.05	0.27	0.08	0.31	0.10
Mn	0.16	0.05	0.17	0.05	0.17	0.05	0.18	0.06	0.18	0.06
S	23.1	7.13	25.1	7.75	21.29	6.57	18.6	5.74	18.29	5.65
SG	24.41	7.53	22.58	6.97	27.75	8.56	25.61	7.90	26.37	8.14
Wd	8.62	2.66	7.88	2.43	7.11	2.19	8.12	2.51	7.91	2.44
Sb	1.55	0.48	1.56	0.48	1.53	0.47	1.43	0.44	1.38	0.43
B	43.62	13.46	43.81	13.52	43.43	13.40	44.09	13.61	43.27	13.35
M	33.11	10.22	33.04	10.20	32.24	9.95	33.34	10.29	33.2	10.25
L	14.91	4.60	14.86	4.59	14.55	4.49	14.67	4.53	14.26	4.40
Ws	3.21	0.99	3.05	0.94	3.26	1.01	3.3	1.02	3.39	1.05
W	170.83	52.73	170.99	52.77	170.73	52.69	170.73	52.69	170.67	52.68
Total	324.00	100.00	324.00	100.00	324.00	100.00	324.00	100.00	324.00	100.00

Table 6. Accuracy of the classified LULC images of Quseir (1984-2021)

LULC	19 84		19 94		20 01		20 13		20 21	
	UA	PA	UA	PA	UA	PA	UA	PA	UA	PA
Ur	100.00	100.00	100.00	90.91	94.44	94.44	96.55	93.33	91.43	88.89
Gr	0	0	90.91	90.91	92.31	92.31	93.33	93.33	93.33	93.33
Mn	100.00	100.00	90.91	90.91	90.91	90.91	92.31	92.31	92.31	92.31
S	88.00	91.67	91.84	93.75	88.00	91.67	90.20	95.83	90.00	95.74
SG	87.10	88.52	87.50	93.33	87.10	90.00	90.00	88.52	89.66	85.25
Wd	88.68	88.68	90.38	88.68	90.20	86.79	91.84	84.91	92.16	88.68
Sb	93.94	93.94	91.18	93.94	91.18	93.94	94.12	96.97	100.00	100.00
B	95.38	91.18	95.38	91.18	96.97	94.12	91.43	94.12	88.73	92.65
M	93.94	91.18	91.43	94.12	91.43	94.12	94.12	94.12	91.43	94.12
L	92.31	96.00	95.83	92.00	95.83	92.00	92.00	92.00	100.00	96.00
Ws	93.94	91.18	91.43	94.12	94.12	94.12	96.97	94.12	100.00	100.00
W	93.75	95.74	95.56	91.49	93.48	91.49	95.83	97.87	100.00	100.00
OA	91.83		92.22		91.90		93.84		94.70	
K C	0.8782		0.8918		0.8812		0.8942		0.9022	

UA= User Accuracy, PA= Producer accuracy, OA= Overall accuracy, KC= Kappa Coefficient

3.1.2. Sigmoid kernel in SVM

For the current work, Sigmoid kernel achieved the highest classification accuracy results by 91.83, 92.22, 91.90, 93.84, and 94.70 %, for Quseir LULC in 1984, 1994, 2001, 2013 and 2021, which are corresponding to Kappa statistics equal to 0.8782, 0.8918, 0.8812, 0.9024 and 0.9128, respectively (Table 6). In general, SVMs are among the top classifiers mainly due to its ability to handle the problems of high dimensionality and limited training samples (Sheykhmousa et al., 2019). The performance of the SVM method depends on the suitable selection of a kernel. The most common procedure for SVM best kernel selection is the trial-and-error approach (e.g., Ali and Smith, 2008). Achieving high accuracy results by Sigmoid kernel in this study is in agreement with Hawash et al., 2021a, who used four SVM kernels to classify Port Sudan with twenty LULC categories, where sigmoid, achieved the highest accuracy results.

3.2. LULC change of Quseir, 1984-2021.

In change detection analysis, differences in areas between the studied intervals represent the final (fixed) quantities that do not explain where the losses go or where the gains come from, which can be overcame by using PCC cross tabulation. Cross tabulation extracted from PCC is the detailed quantitative path that determines the converted area from a specific category to another/others during the investigated interval.

To easily analyse the change outputs, results will be presented in three sections: (i) desert categories (i.e. RSH, sandy areas, and mixed sand and gravel, etc.), (ii) coastal categories (i.e. mangrove, coastal sabkha and water) and (iii) urban categories (i.e. green areas and mixed urban/built-up areas) (Tables 7-10).

Desert land cover categories of the RSCC are very important environmentally and economically (e.g. Elnaggar et al., 2020; Gaafar et al., 2016; Hawash et al., 2021 b; Nasr, 2015; Yousif and Sracek, 2016). Categories of the RSH (i.e. Basalt, metamorphic, limestone) in Quseir had almost the same areas throughout the resulted maps of the studied dates (Fig 3-4) (Table 5). The small changes occurred in the basaltic, metamorphic or limestone rocks of the area may be referred to the classification conditions. Further, most of the changes related to areas covered by sandy areas or mixed sand and basalt (gravel) areas

Table 7. LULC conversion matrix of Quseir between 1984 and 1994.

	Ur	Gr	Mn	S	SG	Wd	Sb	B	M	L	Ws	W	Total, 1994
Ur	0.47	0	0	0.09	0.27	0.02	0	0	0	0	0	0	0.85
Gr	0	0	0	0.09	0.01	0.01	0	0	0	0	0	0	0.11
Mn	0	0	0.16	0	0	0	0.01	0	0	0	0	0	0.17
S	0	0	0	20.91	4.06	0.12	0	0.01	0	0	0	0	25.1
SG	0	0	0	1.82	19.92	0.75	0	0.03	0	0.06	0	0	22.58
Wd	0.01	0	0	0.11	0.03	7.71	0	0	0.02	0	0	0	7.88
Sb	0	0	0	0.02	0	0	1.54	0	0	0	0	0	1.56
B	0	0	0	0.06	0.11	0.01	0	43.58	0.03	0.02	0	0	43.81
M	0	0	0	0	0	0	0	0	33.04	0	0	0	33.04
L	0	0	0	0	0.01	0	0	0	0.02	14.83	0	0	14.86
Ws	0	0	0	0	0	0	0	0	0	0	3.03	0.02	3.05
W	0	0	0	0	0	0	0	0	0	0	0.18	170.81	170.9
Total, 1984	0.48	0	0.16	23.1	24.41	8.62	1.55	43.62	33.11	14.91	3.21	170.83	324.0

Table 8. LULC conversion matrix of Quseir between 1994 and 2001.

	Ur	Gr	Mn	S	SG	Wd	Sb	B	M	L	Ws	W	Total 2001
Ur	0.84	0	0	0.33	0.51	0	0	0	0	0.11	0	0	1.79
Gr	0	0.11	0	0.03	0.01	0	0	0	0	0	0	0	0.15
Mn	0	0	0.17	0	0	0	0	0	0	0	0	0	0.17
S	0	0	0	18.99	1.44	0.01	0.02	0	0.77	0.06	0	0	21.29
SG	0	0	0	5.25	19.82	1.65	0.01	0.78	0.07	0.17	0	0	27.75
Wd	0	0	0	0.42	0.61	5.79	0.01	0.26	0.01	0.01	0	0	7.11
Sb	0	0	0	0.01	0	0	1.52	0	0	0	0	0	1.53
B	0	0	0	0.09	0.08	0.38	0	42.75	0.06	0.07	0	0	43.43
M	0	0	0	0.04	0.03	0.01	0	0.01	32.12	0.03	0	0	32.24
L	0.01	0	0	0.05	0.06	0.01	0	0	0.01	14.41	0	0	14.55
Ws	0	0	0	0	0	0	0	0.01	0	0	2.97	0.28	3.26
W	0	0	0	0	0	0	0	0	0	0	0.02	170.71	170.7
Total, 1994	0.85	0.11	0.17	25.21	22.56	7.85	1.56	43.81	33.04	14.86	2.99	170.99	324.0

Ur= Mixed urban/built-up areas, Gr= Green area, Mn= Mangrove, S= Sandy areas other than beaches, SG= Mixed sand and gravel, Wd= Wadi deposits, Sb= Coastal sabkha, B= Basalt, M= Metamorphic, L= Limestone, Ws= Shallow water and W= Water.

Table 9. LULC conversion matrix of Quseir between 2001 and 2013.

	Ur	Gr	Mn	S	SG	Wd	Sb	B	M	L	Ws	W	Total, 2013
Ur	1.77	0	0	0.31	0.99	0.52	0	0.02	0.05	0	0	0	3.66
Gr	0	0.15	0	0.05	0.03	0.04	0	0	0	0	0	0	0.27
Mn	0	0	0.17	0	0	0	0.01	0	0	0	0	0	0.18
S	0	0	0	16.61	1.75	0.02	0.05	0	0.09	0.08	0	0	18.6
SG	0	0	0	1.4	22.45	0.51	0.03	0.52	0.31	0.39	0	0	25.61
Wd	0	0	0	2.02	0.83	5.11	0.03	0.13	0	0	0	0	8.12
Sb	0	0	0	0.01		0	1.41	0	0	0	0.01	0	1.43
B	0	0	0	0	0.67	0.99	0	42.42	0.01	0	0	0	44.09
M	0	0	0	0.42	0.86	0.01	0	0.31	31.71	0.03	0	0	33.34
L	0.01	0	0	0.35	0.16	0.01	0	0.01	0.07	14.06	0	0	14.67
Ws	0.01	0	0	0	0	0	0	0.03	0	0	3.23	0.03	3.3
W	0	0	0	0	0	0	0	0	0	0	0.02	170.71	170.7
Total, 2001	1.79	0.15	0.17	21.17	27.74	7.21	1.53	43.44	32.24	14.56	3.26	170.74	324.0

Table 10. LULC conversion matrix of Quseir between 2013 and 2021.

	Ur	Gr	Mn	S	SG	Wd	Sb	B	M	L	Ws	W	Total, 2021
Ur	3.65	0	0	0	0.44	0.41	0.02	0.06	0.09	0.10	0	0	4.77
Gr	0	0.26	0	0.02	0.01	0.02	0	0	0	0	0	0	0.31
Mn	0	0	0.18	0	0	0	0	0	0	0	0	0	0.18
S	0	0	0	15.72	2.4	0.02	0	0.04	0.03	0.08	0	0	18.29
SG	0	0	0	2.75	22.39	0.15	0.01	0.83	0.07	0.17	0	0	26.37
Wd	0.01	0	0	0.14	0.28	7.43	0.01	0.01	0	0.03	0	0	7.91
Sb	0	0	0	0	0	0	1.38	0	0	0	0	0	1.38
B	0	0	0	0	0.04	0.05	0.01	43.15	0.02	0	0	0	43.27
M	0	0	0	0.01	0.01	0	0	0	33.11	0.07	0	0	33.2
L	0	0	0	0.01	0.01	0	0	0	0.02	14.22	0	0	14.26
Ws	0	0.01	0	0	0	0	0	0	0	0	3.29	0.09	3.39
W	0	0	0	0	0	0	0	0	0	0	0.01	170.66	170.6
Total, 2013	3.66	0.27	0.18	18.65	25.58	8.08	1.43	44.09	33.34	14.67	3.3	170.75	324.0

Ur= Mixed urban/built-up areas, Gr= Green area, Mn= Mangrove, S= Sandy areas other than beaches, SG= Mixed sand and gravel, Wd= Wadi deposits, Sb= Coastal sabkha, B= Basalt, M= Metamorphic, L= Limestone, Ws= Shallow water and W= Water.

were mainly referred to natural and/or meteorological conditions that affected the RSCC during the 1990s-2010s. Flash floods hit areas along the Red Sea coast on different occasions during the last four decades. In particular, flash floods hit populated areas and main road network of Ras Gharib, Hurghada, Safaga, Quseir and Marsa Alam (e.g., Abdel Fattah, 2015; Bauer et al., 2020; Elnazer et al., 2017) that caused major economic and anthropogenic loss as well as transferring sand and gravel from an area to another.

According to National Ocean Service, salt marshes, mangroves, and seagrass beds absorb large quantities of the greenhouse gas carbon dioxide from the atmosphere and store it, thus decreasing the effects of global warming. For their ecological and socio-economic rules, monitoring mangroves, sabkha and other coastal resources is very important, even if they have small areas.
Mangroves in Egypt occupy 5.25 km^2 (Zahran and Willis 2009; Afefe, 2021). In this study, mangrove located in two main areas, the first is to the north and the second is to the south of the city centre. In 1984, mangroves area was 0.16 km^2, which ended by 0.18 km^2 in 2021. This increase may be explained by "non influenced areas by anthropogenic activities", or because of the soil properties of the area that suit this mangrove (*Avicennia marina*) (e.g., Sheded et al.,2013; Basheer et al., 2019). Recently, six sites suitable for mangroves plantation were identified along Quseir-Marsa Alam corridor by Abd-El Monsef et al., 2017.

Along the study period, northern coastal sabkha was increased by 0.04 km^2, while the southern coastal sabkha was decreased by 0.22 km^2 (Tables 7-10). From field visits, the northern region had no evidence of anthropogenic influences, which indicate natural increase. Meanwhile, the southern region was filled with construction waste in preparation for its urban development, which is shown to have an adverse impact on the region in future (e.g., Alnuaim and El Naggar, 2014; Aqeel, 2016).

The changes occurred between the shallow water and sea water categories are very limited and may be referred to classification conditions. Further, there were no evidences of changes between the land categories and water categories through land fill or dredging like those occurred in Hurghada, north Red Sea (e.g., Dewidar, 2002; Kamh et al., 2012; Vanderstraete et al., 2006).

Meanwhile, an in-depth study is needed to investigate the land-water changes of the region and the natural long shore sedimentation and alongshore processes.

From the classified images and information obtained from the locals, there were no green areas in Quseir in 1984. But, in 1994, green areas began to appear and increase from 0.11 to 0.15, 0.27 and 0.31 km^2 with growth rate of 36.40, 80.00 and 14.80 % during the second, third and fourth interval, respectively. Of the 0.31 km^2 of growth in green areas (1994- 2021), more than 50% were converted from sand, 22% from mixed sand and gravel and 23% from wadi deposits, and the remained area was converted from other LULC types. When comparing the area of green areas with the population number of Quseir in 2020, the share of the green areas is 6.40 m^2/person. This area is more than (2/3) the area recommended by World Health Organisation (WHO) (i.e. 9.00 m^2/person) (Morar et al., 2014; Maryanti et al., 2016). A big share of the green areas is located in the touristic villages of the study area.

Urban of Quseir was 0.48 km^2 in 1984. Then, it was increased by an area of 0.37, 0.94, 1.87 and 1.11 km^2 during the first, second, third and fourth interval, respectively (Figure 3-4), (Tables 7-10). Along 1984-2021, the relative change of the urban was about 894.00%, which represent 24.00 % annual growth rate (a.g.r.). The greatest increase was during the second interval of about 110.00% (15.80% a.g.r.) and the lowest increase was during the fourth interval of about 30.00% (3.00% a.g.r.). Along the study period, most of the urban area was expanded in the northern areas of the old city and over deserted land covers. Of the total 4.29 km^2 urban growth, about 55.00% were converted from mixed sand and gravel, 26.00% from sandy areas, 13.00% from wadi deposits and the remained 6.00% were converted from other LULC types.

4. CONCLUSION

Mapping LULC and extracting LULC changes of coastal cities can be effectively obtained using remote sensing and GIS. Using four Landsat datasets and a Sentinel-2 image cover the period from 1984-2021, SVM classifier and PCC change detection technique were direct and time and cost efficient in obtaining LULC change information of a desert semi-arid coastal city like Quseir. This study produced some important numbers as follows, urban was increased by about nine folds (over desert areas); urban green area was

increased from nil to more that 6.4 m^2/person (most of the green area is located in touristic villages); mangroves area was naturally increased by more than 12.0% (no anthropogenic disturbance); and the coastal sabkha was decreased by 12% (landfill activities). The information identified by this study will contribute well in managing the city and its surrounding. To get a full spatial view of Quseir, it is important to conduct land-water change study at the city's coast covering the past four decades.

ACKNOWLEDGMENTS

The authors would like to thank the anonymous reviewers for their thoughtful and detailed comments, which have improved the manuscript.

REFERENCES

Abdel-Aal, A., M. (1992). New towns and regional development in Egypt. Arts and human sciences magazine, Minia university, 10 (2): 71-135.

Abdel-Fattah, M., Kantoush, S. and Sumi, T. (2015). Integrated Management of Flash Flood in Wadi System of Egypt: Disaster Prevention and Water Harvesting. In: Annuals of Disas. Prev. Res. Inst., Kyoto Univ., 58 (B): 485-496.

Abdel Ghany, M.K. (2015). Quantitative Morphometric Analysis of Drainage Basins between Qusseir and Abu Dabbab Area, Red Sea Coast, Egypt using GIS and Remote Sensing Techniques, International Journal of Advanced Remote Sensing and GIS, 4(1): 1295-1322.

Abd-El Monsef, H., Hassan, M.A.A. and Shata, S. (2017). Using spatial data analysis for delineating existing mangroves stands and siting suitable locations for mangroves plantation. Comput Electron Agric 141: 310–326

Abe, S. (2005). Support Vector Machines for Pattern Classification. 2nd Ed, Springer, 471p.

Adler-Golden, S. M., M. W. Matthew, L. S. Bernstein, R. Y. Levine, A. Berk, S. C. Richtsmeier, P. K. Acharya, G. P. Anderson, G. Felde, J. Gardner, M. Hoke, L. S. Jeong, B. Pukall, A. Ratkowski, and H.-H Burke (1999). Atmospheric Correction for Short-wave Spectral Imagery Based on MODTRAN4. JPL Publ., 99(17): 21-29.

Afefe, A.A. (2021). Linking territorial and coastal planning: Conservation status and management of mangrove ecosystem at the Egyptian - African Red Sea coast. Aswan University Journal of Environmental Studies, 2(2): 91-114

Ali, S. and Smith, K.A. (2008). Kernel Width Selection for SVM Classification: A Meta-Learning Approach. In: Felici, G. and Vercellis, C. (Eds.), Mathematical Methods for Knowledge Discovery and Data Mining, Information science reference, Hershey, New York, 101-115.

Aljenaid, S.S., Kadhem, G.R., AlKhuzaei, M.F. and Alam, J.B. (2022). Detecting and assessing the spatio-temporal land use land cover changes of Bahrain Island during 1986–2020 using remote sensing and GIS. Earth Systems and Environment, https://doi.org/10.1007/s41748-022-00315-z

Alawamy, J.S., Balasundram, S., Hanif, A.H.M. and Teh, C.B.S. (2020). Detecting and Analyzing Land Use and Land Cover Changes in the Region of Al-Jabal Al-Akhdar, Libya Using Time-Series Landsat Data from 1985 to 2017. Sustainability, 12, 4490. DOI: 10.3390/su12114490.

Anderson, R., Hardy, E.E., Roach, J.T., & Witmer, R.E. (1976). A land use and land cover classification system for use with remote sensor data. Sioux Falls: US Gov. Printing Office.

Al-doski, J., Mansor, S.B. and Shafri, H.Z.M. (2013). Image Classification in Remote Sensing. Journal of Environment and Earth Science, 3, 10.

Alganci, U. (2019). Dynamic Land Cover Mapping of Urbanized Cities with Landsat 8 Multi-temporal Images: Comparative Evaluation of Classification Algorithms and Dimension Reduction Methods. Int. J. Geoinf , 8(3):139.

Alnuaim, A.M. and El Naggar, M. H. (2014). Performance of Foundations in Sabkha Soil: Numerical Investigation. Geotech Geol Eng, 32:637–656

Aqeel, A. (2016). Investigation of expansive soils in Obhor Sabkha, Jeddah-Saudi Arabia. Arab J Geosci, 9, 314

Basheer, M.A., El Kafrawy, S.B. and Mekawy, A.A. (2019) Identification of mangrove plant using hyperspectral remote sensing data along the Red Sea, Egypt. Egyptian Journal of Aquatic Biology & Fisheries, 23(1): 27 – 36.

Bauer, F., Hadidi, A., Tügel, F. and Hinkelmann, R. (2020). Flash Flood Investigations in El Gouna, Northern Red Sea Governorate, In: A. M. Negm (ed.), Flash Floods in Egypt, Advances in Science, Technology & Innovation. Springer Nature Switzerland AG, 61-81.

Cabassi, A. (2012). Kosseir, a phosphate-shipping town. In Piaton, C., Godoli, E. and Peyceré, D.(Eds.). BUILDING BEYOND THE MEDITERRANEAN: Studying the archives of European businesses (1860-1970), 104-117. Arles, Publications de l'Institut national d'histoire de l'art, InVisu (CNRS-INHA), Honoré Clair. DOI : 10.4000/books.inha.12579

CAPMAS, 2021. Population Statistics and Censuses Sector PSCS, Central Agency for Public Mobilization and Statistics, Census - Population (governorates), Imtedad Ramsis, Cairo.

Cavur, M., Duzgun, H.S., Kemec, S. and Demirkan, D. C. (2019). Land use and land cover classification of Sentinel 2-a: st Petersburg case study. Int. Arch. Photogramm. Remote Sens. Spat. Inf. Sci.Vol. XLII-1/W2.

Chan, J.C., Chan, K., Yeh, A.G. (2001) Detecting the Nature of Change in an Urban Environment: a Comparison of Machine Learning Algorithms. Photogramm Eng Remote Sensing, 67(2):213–225

Chander, G., Markham, B.L., Helder, D.L., 2009. Summary of current radiometric calibration coefficients for Landsat MSS, TM, ETM+, and EO-1 ALI sensors. Remote Sens. Environ. 113, 893–903.

Chughtai, A.H., Abbasi, H. and Karas, I.R. (2021). A review on change detection method and accuracy assessment for land use land cover. Remote Sens. Appl.: Soc. Environ. 22:100482

Chuvieco, E. (2020) Fundamentals of Satellite Remote Sensing: An Environmental Approach, 3rd ed., CRC press, 432p.

Congalton, R. G., & Green, K. (2019). Assessing the accuracy of remotely sensed data: Principles and practices (3rd ed., p. 327). CRC Press.

Dewidar, Kh. (2002). Landfill detection in Hurghada, North Red Sea, Egypt, using Thematic Mapper images. Int. J. Remote Sens., 23(5): 939–948.

EGSMA, 1991. Basement Rocks of Quseir Quadrangle, Egypt (sheet No. NG-36-NE). Ministry of Petroleum and Mineral Resources, The Egyptian Geological Survey and Mining Authority.

Elnaggar, O.M. Temraz, M.G. and Khallaf, M.K. (2020). Detection of flow units of Quseir Formation (Lower Campanian) as a potential reservoir using experimental correlations of capillary pressure derived parameters, Gebel el-Silsila, Egypt. Journal of Petroleum Exploration and Production Technology, 10: 2269–2277

Elnazer, A. A., Salman, S. A. and Asmoay, A. S. (2017). Flash flood hazard affected Ras Gharib city, Red Sea, Egypt: a proposed flash flood channel. Nat. Hazards, 89:1389-1400.

EMA (2016). Meteorological data of Qusair and Ras Banas 1986-2016. Egyptian Meteorological Authority, Kobry elQobba, AlWaili, Cairo, 11784.

ENVI GCD. L3Harris Geospatial documentation center. Support Vector Machine. Available online:

https://www.harrisgeospatial.com/docs/SupportVectorMachine.html (accessed: 30 May, 2022)

ESA (2008). Topographic map of Quseir, Egypt, sheet number (NG-36-K3), Ministry of Water Resources and Irrigation, Egyptian Survey Authority.

Foody, G. M. and Mathur, A. (2004). Toward intelligent training of supervised image classifications: directing training data acquisition for SVM classification. Remote Sens. Environ., 93 (1-2): 107–117.

Gaafar, I., El-Shershaby, A., Zeidan, I. and Sayed El-Ahll, L. (2016). Natural radioactivity and radiation hazard assessment of phosphate mining, Quseir-Safaga area, Central Eastern Desert, Egypt. NRIAG Journal of Astronomy and Geophysics, 5(1): 160-172.

Green, K., Kempka, D. and Lackey, L. (1994). Using remote sensing to detect and monitor land-cover and land-use change. Photogramm. Eng. Remote Sens., 60: 331–337

Hawash, E. (2014). Monitoring changes of Rosetta, North-west Nile delta, Egypt, 1983-2013. Annual Conference, Possible Impacts of Climate Change on Africa, Institute of African Research and Studies, Cairo Univ., 18-20 May, 2014. Available at: https://cu.edu.eg/userfiles/abstractsfinal.pdf (Accessed: 4 May 2022).

Hawash, E., El-Hassanin, A., Amer, W., El-Nahry, A. and Effat, H. (2021a). Change detection and urban expansion of Port Sudan, Red Sea, using remote sensing and GIS. Environ Monit Assess, 193,723. DOI: 10.1007/s10661-021-09486-0 .

Hawash, E., El-Hassanin, A., Amer, W., El-Nahry, A. and Effat, H. (2021b). Land use land cover change of Marsa Alam, Red Sea, using remote sensing and GIS. MISJ, 1(2): 148-166. DOI: 10.21608/misj.2021.196443 .

Huang, C., Davis, L. S., & Townshend, J. R. G. (2002). An assessment of support vector machines for land cover classification. Int J Remote Sens, 23(4): 725–749.

Ihlen, V., 2019. Landsat 8 (L8) data users handbook (US geological survey, sioux falls, south Dakota). https://www.usgs.gov/core-science-systems/nli/landsat/landsat-8-data-users-handbook. Accessed 14 Oct. 2021.

Ilsever, M. and Ünsalan, C. (2012). Two-Dimensional Change Detection Methods, Remote Sensing Applications. Springer, 72p.

Izadi, F., Chamani, A. and Zamani-Ahmadmahmoodi, R. (2022). How vegetation cover characteristics response to the spread of Prosopis juliflora:

a time-series remote sensing analysis in southern Iran. Environ Monit Assess, 194: 401.26

Jensen, J. R. (2005). Introductory digital image processing. 3rd ed., Prentice Hall, 526p.

Jensen, J. R. (2015). Introductory digital image processing. 4th ed., Pearson Education, 656p.

Jumaah, H.J., Ameen, M.H., Mohamed, G.H. and Ajaj, Q.M.(2022). Monitoring and evaluation Al-Razzaza lake changes in Iraq using GIS and remote sensing technology. Egypt. J. Remote. Sens. Space Sci, 25 (1): 313-321

Kamel, M. and Abu El Ella, E.M. (2016). Integration of remote sensing and GIS to manage the sustainable development in the Nile Valley desert fringes of Assiut-Sohag Governorates, Upper Egypt. J Indian Soc Remote Sens, 44(5):759–774

Kamh, S., Ashmawy, M., Kilias, A., and Christaras, B. (2011). Evaluating urban land cover change in the Hurghada area, Egypt, by using GIS and remote sensing. Int J Remote Sens, 33(1): 41-68.

Keuchel, J., Naumann, S., Heiler, M. & Siegmund, A. (2003). Automatic land cover analysis for Tenerife by supervised classification using remotely sensed data. Remote Sens. Environ., 86 (4): 530-541.

Lambin, E.F., Geist, H.J. and Rindfuss, R.R. (2014). Introduction: Local Processes and Global Impacts, In: Eric F. Lambin, E.F. and Geist, H.J. (Eds), Land-Use and Land-Cover Change: Local Processes and Global Impacts, Springer, 1-8.

Lambert, M. J., Traoré, P. G. S., Blaes, X., Baret, P. and Defourny, P. (2018). Estimating smallholder crops production at village level from Sentinel-2 time series in Mali's cotton belt, Remote Sens. Environ., 216: 647–657.

Lillesand, T. M., R. W. Kiefer and J. W. Chipman (2015). Remote Sensing and Image Interpretation, 7th Edition. John Wiley & Sons, Inc., New York, New York, 720 p.

Lu, D., Mausel, P., Brondízio, E. and Moran, E. (2004). Change detection techniques. Int J Remote Sens, 25 (12): 2365-2407.

Lu, D., and Weng, Q. (2007). A survey of image classification methods and techniques for improving classification performance. Int J Remote Sens, 28(5): 823–870.

Lunetta, R.S. (2000). Remote Sensing Change Detection. 1st Ed. CRC, 350p.

Main-Knorn, M., Pflug, B., Louis, J., Debaecker, V., Müller-Wilm, U., Gascon, F. (2017). Sen2Cor for Sentinel-2. 3. Conference of Image and Signal Processing for Remote Sensing. DOI: 10.1117/12.2278218.

Mandal, J., Ghosh, N. and Mukhopadhyay, A. (2019). Urban Growth Dynamics and Changing Land-Use Land-Coverof Megacity Kolkata and Its Environs. J. Indian Soc. Remote Sens., 47, 1707–1725

Mansour, A.M., Nawar, A.H. and Madkour, H.A. (2011). Metal pollution in marine sediments of selected harbours and industrial areas along the Red Sea coast of Egypt. Ann. Naturhist. Mus. Wien, Serie A, 113: 225–244

Maryanti, M. R., Khadijah, H., Uzair, A.M. and Ghazali, M.A. (2016). The urban green space provision using the standards approach: issues and challenges of its implementation in Malaysia, Sustainable Development and Planning VIII, WIT Trans. Ecol. Environ., 210: 369-379.

MoHUUC (2014). The National Urban Development Framework in the Arab Republic of Egypt. Report presented by the Ministry of Housing, Utilities and Urban Communities, General Organization for Physical Planning (GOPP), Egypt.

Morar, T., Radoslav, R., Spiridon, L. C., and Păcurar, L. (2014). Assessing pedestrian accessibility to green space using GIS. Transylvanian Rev. Adm. Sci., 10(42): 116–139.

Nasr, A.M.A. (2015). Geotechnical Characteristics of Stabilized Sabkha Soils from the Egyptian–Libyan Coast. Geotech Geol Eng, 33:893–911

National Ocean Service (without date). Coastal Blue Carbon. National Oceanic and Atmospheric Administration-NOAA. Available at: https://oceanservice.noaa.gov/ecosystems/coastal-blue-carbon/ (Accessed: 4 March, 2022).

Peiman, R. (2011). Pre-classification and post-classification change-detection techniques to monitor land-cover and land-use change using multi-temporal Landsat imagery: a case study on Pisa Province in Italy. Int J Remote Sens, 32 (15): 4365-4381.

Richards, J. A. (2013). Remote Sensing Digital Image Analysis: An Introduction, 5th Ed. Springer Heidelberg New York, London, 494 p.

Said, R. (1992). The Geology of Egypt, Elsevier Science Ltd., 1st Edition. Rotterdam, Netherlands, 734 p.

Salem, A., Aboud, E., Elsirafy, A. and Ushijima, K. (2005). Structural mapping of Quseir area, northern Red Sea, Egypt, using high-resolution aeromagnetic data, Earth Planets Space, 57: 761–765.

Sheded M. G.; Ahmed M. K. and Hammad S. A. (2013). Vegetation Analysis in the Red Sea-Eastern Desert ecotone at the area between Safaga and South Qusseir, Egypt. Helwan Conf. Egypt J Bot. 3rd Int. Conf. 17-18, Helwan Univ. 145-163.

Sheykhmousa, M., Kerle, N., Kuffer, M. and Ghaffarian, S. (2019). Post-disaster recovery assessment with machine learning-derived land cover and land use information, Remote Sens., 11, 10, 1174.

Singh, A. (1989). Digital change detection techniques using remotely sensed data. Int J Remote Sens, 10: 989–1003.

Singh, S.K., Kanga, S., Meraj, G., Farooq, M. and Sudhanshu (2021). Geographic Information Science for Land Resource Management, 1st ed., John Wiley & Sons, Inc. York, New York, 406 p.

Steffen, W.L. (2004). Global Change and the Earth System: A Planet Under Pressure. Springer, 336p.

Stow, D. A., Tinney, L. R., & Estes, J. E. (1980). Deriving land use/land cover change statistics from Landsat: A study of prime agricultural land. Proceedings of the 14th International Symposium on Remote Sensing of Environment held in Ann Arbor in 1980 (Ann Arbor, Michigan: Environmental Research Institute of Michigan), 1227–1237.

Srivastava, P.K., Han, D., Rico-Ramirez, M.A., Bray, M. and Tanvir Islam (2012). Selection of classification techniques for land use/land cover change investigation. Adv. Space Res. 50: 1250–1265

Turner II, B.L., Moss, R.H. and Skole., D. L. (1993). Relating Land Use and Global Land-Cover Change. International Geosphere-Biosphere Program, Report No. 24/HDP, Report No. 5, Stockholm., Sweden.

USGS (2019a). USGS EROS Archive - Sentinel-2 - Comparison of Sentinel-2 and Landsat. Earth Resources Observation and Science (EROS) Centre. Available online: https://www.usgs.gov/centers/eros/science/usgs-eros-archive-sentinel-2-comparison-sentinel-2-and landsat#:~:text=The%20main%20visible%20and%20near,spatial%20resolution%20of%2060%20meters (Accessed: Oct., 28, 2022.

USGS (2019b). Landsat 8 (L8) Data Users Handbook. LSDS-1574 Version 5.0, USGS. Available online: https://d9-wret.s3.us-west-

2.amazonaws.com/assets/palladium/production/s3fs-public/atoms/files/LSDS-1574_L8_Data_Users_Handbook-v5.0.pdf (Accessed: Oct., 28, 2022).

USGS (2019c). USGS EROS Archive - Sentinel-2, USGS. Available online: https://www.usgs.gov/centers/eros/science/usgs-eros-archive-sentinel-2 (Accessed: Oct., 28, 2022).

Vanderstraete, T., Goossens, R., & Ghabour, T. K. (2006). The use of multi-temporal Landsat images for the change detection of the coastal zone near Hurghada Egypt. Int. J. Remote Sens., 27(17): 3645–3655.

Vapnik., V. (1995). The Nature of Statistical Learning Theory. Springer, New York, 188 p.

Verburg, P. H., Neumann, K. and Nol, L.(2011). Challenges in using land use and land cover data for global change studies. Glob. Change Biol., 17: 974–989.

Walker, B. and Steffen, W. (1999). The nature of global change, In: Walker, B., Steffen, W., Canadell, J. and Ingram, J. (Eds.), The Terrestrial Biosphere and Global Change: Implications for natural and managed, ecosystems, International Geosphere-Biosphere Programme Book Series, 1–18

Youssef, A. M., Pradhan, B., Gaber, A. F. D. and Buchroithner, M. F. (2009).Geomorphological hazard analysis along the Egyptian Red Sea coast between Safaga and Quseir. Nat. Hazards Earth Syst. Sci., 9: 751–766.

Yousif, M. and Sracek, O. (2016). Integration of geological investigations with multi-GIS data layers for water resources assessment in arid regions: El Ambagi Basin, Eastern Desert, Egypt, Environ. Earth Sci., 75: 684.

Yuan, D., Elvidge, C.D. and Lunetta, R.S. (1998) Survey of Multispectral Methods for Land Cover Change Analysis. In: Lunetta, R.S. and Elvidge, C.D., Eds., Remote Sensing Change Detection: Environmental Monitoring. Methods and Application, Taylor and Francis Ltd., 21-39.

Zahran M. and Willis A. (2009). The vegetation of Egypt. 2nd ed., Springer, 456 p.

Zhang, R., Tang, X., You, S., Duan, K., Xiang, H. and Luo, H. (2020). A novel feature-level fusion framework using optical and SAR remote sensing images for land use/land cover (LULC) classification in cloudy mountainous area. Appl. Sci., 10, 8: 2928.

لقط و رسم خرائط الغطاء الأرضي - استخدامات الأراضي و رصد التغييرات بالاستناد علي SVM باستخدام بيانات لاندسات و سينتينيل-٢. حالة القصير ، البحر الأحمر.

عماد حواش
دكتوراه- قسم الموارد الطبيعية
كلية الدراسات الأفريقية العليا، جامعة القاهرة، الجيزة ، مصر
مركز البحر الأحمر لدراسات الأستدامة
al_hawash@yahoo.com

أ.د./ **عادل الحسنين**
قسم الموارد الطبيعية
كلية الدراسات الأفريقية العليا، جامعة القاهرة

أ.د. **وفاء عامر**
قسم التخطيط العمراني
كلية التخطيط الإقليمي والعمراني، جامعة القاهرة

أ.د. **علاء الدين النهري**
شعبة التدريب والتعليم المستمر
الهيئة القومية للاستشعار من بعد وعلوم الفضاء
وزارة البحث العلمي

أ.د. **هالة عفت**
شعبة البيئة و استعمالات الاراضي
الهيئة القومية للاستشعار من بعد وعلوم الفضاء
وزارة البحث العلمي

المستخلص:
يعد رسم خرائط استخدامات-الغطاء الأرضي ورصدالتغيرات المكانية ضروريين لإدارة المدن الساحلية. تهدف هذه الدراسة إلى التحقيق في تغيرات استخدامات - الغطاء الأرضي في القصير ، وهي نموذج لمدينة ساحلية صغيرة على البحر الأحمر، خلال فترة زمنية طويلة ١٩٨٤- ٢٠٢١. تم استخدام مُصنِّف (Support vector machines-SVM) وتقنية (Post classification comparison-PCC) للكشف عن التغيرات لتحليل مرئيتين فضائيتين (TM) ، مرئية فضائية (ETM) و مرئية فضائية (OLI) لاندسات بالاضافة الي مرئية (MSI) سينتينيل-٢ تغطي فترة الدراسة. تم تحديد اثني عشر فئة لاستخدامات - الغطاء الأرضي لهذه الدراسة. تم حساب دقة الصور المصنفة و التغيرات في استخدامات -الغطاء الأرضي. على مدار السبعة والثلاثين عامًا ، ازدادت المناطق الحضرية في القصير بمقدار تسعة أضعاف ، وزادت المساحة الخضراء من صفر إلى ١٠. ٦ مترًا مربعًا للفرد . حقق SVM نتائج تصنيف عالية الدقة لجميع الصور المدروسة لجميع المستشعرات ، بينما كانت الصورة MSI، 2021 ، الأعلى دقة. من خلال إعادة ترتيب الدقة المكانية، أدى الجمع بين بيانات المرئيات الفضائية لاندسات و سينتينيل-٢ لدراسات الرصد طويلة المدى باستخدام (PCC) إلى نتائج أكثر موثوقية و أكثر دقة. سوف تعوض نتائج هذه الدراسة فجوة نقص خرائط استخدامات-الغطاء الأرضي ومعلومات التغييرات المكانية في القصير خلال الاربعة عقود الماضية.

الكلمات الدالة: التغيرات في استخدامات-الغطاء الأرضي ; SVM ; PCC ; لاندسات ; سينتينيل-٢ ; القصير البحر الأحمر.